Detailed Comparative Analysis of Structural Stability and Electron-Phonon Properties of ZrO$_2$:

Mechanism of Water Adsorption on t-ZrO$_2$ (101) and t-YSZ (101) Surfaces

Dilshod Nematov [*] , Amondulloi Burkhonzoda , Kholmirzo Kholmurodov , Andriy I. Lyubchyk , Sergiy Lyubchyk

Keywords: zirconia; stability; yttrium-stabilized zirconia; energy convertion; phase transition; Fermi level shift; water adsorption on the surface

Article

Study on Structural Stability of ZrO2 and YSZ: Doping-Induced Phase Transitions and Fermi Level Shift

D.D. Nematov [1,2,*], A.S. Burkhonzoda [1,2], Kh,T. Kholmurodov [3,4,*], A.I. Lyubchyk [5], S.I. Lyubchyk [5,6] and S.B. Lyubchyk [5,6]

[1] Osimi Tajik Technical University, Dushanbe, 734042 Tajikistan
[2] S.U.Umarov Physical-Technical Institute of   NAS of Tajikistan
[3] Joint Institute for Nuclear Research, Dubna, Moscow Region, 141980 Russia
[4] Dubna State University, Dubna, Moscow Region, 141980 Russia
[5] Universidade Lusofona, 1749-024 Lisboa, Portugal
[6] Faculty of Science and Technology Nova University, Lisbon, Portugal
* Correspondence: dilnem@mail.ru

Abstract: The article deals with the issues of structural stability, electronic properties and phonon dispersion of the cubic, tetragonal and monoclinic phase of ZrO_2. The monoclinic phase of ZrO_2 is found to be the most stable among all the phases of this compound, in terms of total energy comparison, the lowest enthalpy value, the highest entropy and the lowest negative modes found for m-ZrO_2. An analysis of the electronic properties showed that during the m-t phase transformation of ZrO_2, the Fermi level first shifts by 0.125 eV towards higher energies, and then, in the t-c section, goes down by 0.08 eV. In this case, the band gaps for c-ZrO_2, t-ZrO_2, and m-ZrO_2 are 5.14 eV, 5.89 eV, and 5.28 eV, respectively. Calculations based on the analysis of the effect of doping with 3.23, 6.67, 10.35, and 16.15 mol. % Y_2O_3 on the m-ZrO_2 structure showed that the m-YSZ enthalpy decreases linearly, which accompanies doped-induced phase transitions and further stabilization of monoclinic ZrO_2. In this case, the position of the Fermi level changes stepwise, and the energy gap decreases. It has been found that not only for pure systems, including for Y_2O_3-doped systems, the p-states of electrons make the main contributions to the formation of the conduction band. The obtained results complement the database of research works carried out in the field of application of biocompatible zirconium dioxide crystals and ceramics for green energy generation and can be used in the design of humidity-to-electricity converters and the creation of solid oxide fuel cells based on ZrO_2.

Keywords: zirconium dioxide; stability; yttrium-stablized ZrO_2 (YSZ); oxygen vacancy; enthalpy and entropy; doped-induced phase transition; Fermi level shift

1. Introduction

With the ongoing threat of the energy crisis and global warming caused by the increase in the use of fossil energy, the search for sustainable and environmentally friendly sources of energy is one of the most urgent challenges of human civilization in the 21st century [1, 2], since it is known that the continued use of fossil fuels in the world threatens our energy supply and creates a huge burden on the environment. Research on the use of sustainable green energy represents one of the ways to mitigate the growing threat of global environmental problems and the energy crisis, which is very intense and active around the world. Solar panels and wind turbines have become familiar to us. However, new advances in nanotechnology and materials science make it possible to collect energy from other sources and will allow and implement the creative idea of Nikola Tesla about "Getting an electric current from the air" Recently, scientists and engineers have been working on the creation of innovative devices for converting humidity into electricity, which will expand the range of known renewable energy sources due to a new source of atmospheric humidity (galvanic converters that convert air humidity into electricity). That is, such devices are capable of collecting electricity from

atmospheric humidity and supplying electrical current, similar to how solar panels capture sunlight and generate electricity.

Zirconium ceramics have been extensively studied in recent years because of their excellent electrical, optical and mechanical properties. They are also biocompatible and have a wide range of biomedical applications. Tetragonal phase yttria stabilized zirconia (Y-TZP) has been used in various medical applications since the 1980s, particularly for dental crowns [2]. In addition, bulk materials and nanocomposites based on ZrO_2 are used in electrochemical cells because of their high oxide ion conductivity and catalytic activity, low thermal conductivity and mechanical/chemical stability, as well as compatibility with electrolytes, which makes them from a structural point of view [3,4].

One of the most remarkable properties of ceramics based on zirconia is the presence of three crystalline forms with different properties [5–9]. There are the most stable monoclinic (mineral baddeleyite; m-ZrO_2), metastable tetragonal (medium temperature) and unstable cubic structure of zirconium dioxide (high temperature). High-pressure induced zirconium phases in the form of brookite (orthorhombic-I) and cotunnite (orthorhombic-II) are also known [10,11]. Pure zirconium dioxide undergoes a phase transformation from monoclinic to tetragonal (about 1173°C), and then to cubic (about 2370°C), accompanied by a change in volume and, accordingly, their strength [12–14]. For the application of zirconia in advanced zirconia ion-conducting ceramic devices, it is important that the stabilized material has an adequate level of conductivity and the desired mechanical-chemical stability in both oxidizing and reducing atmospheres. Obtaining a stable material from zirconia is difficult due to a noticeable change in volume during the phase transition. Stabilization of zirconium dioxide is achieved by replacing some Zr^{4+} ions with larger ions in the crystal lattice [15–17]. For example, numerous studies have shown that doping with polyvalent oxides, including certain concentrations of yttrium oxide, stabilizes the high-temperature cubic and tetragonal phases of ZrO_2 at room temperature. This also leads to an increase in the concentration of oxygen vacancies and oxygen-ion conductivity, which makes it possible to use stabilized ZrO_2 as an electrolyte in fuel cells [17]). The ionic conductivity of ZrO_2 strongly depends on the phase modification and the content of stabilizing additives in the system, which is also evidenced by the phase diagram given in [18]. At the same time, it is difficult to study experimentally single crystals of pure ZrO_2 grown from a melt, they exhibit phase transformations upon cooling, therefore, their doped structures (for example, yttrium-doped structure ZrO_2, YSZ) are usually studied. However, the surface chemistry of YSZ is much more complex than that of the purest ZrO_2. In another work, Kobayashi et al. [19] found that YSZ decomposes slowly at about 250°C due to the t-m transformation. This t-m transformation is accompanied by microcracking and loss of material strength in a humid atmosphere. This t-m transformation also occurs due to the presence of water or a humid environment in zirconia-based ceramic materials, which is called low-temperature degradation or aging of ZrO_2 crystals. Over the past couple of decades, a large amount of work has been done on this topic, including many hypotheses and discussions, and the most reliable hypothesis on the YSZ topic is based on filling oxygen vacancies that were present in the matrix to maintain a stable t-YSZ phase. Thus, filling these O-vacancies with water radicals, either O_2 or OH, destabilizes the YSZ phase. However, the YSZ stabilization mechanism itself is not fully understood, and it is still the subject of much debate. Therefore, theoretical research and modeling of the properties of bulk and 2D materials based on ZrO_2 and YSZ is necessary as a starting point for a good understanding of their fundamental properties. On the other hand, aspects of the shift of the Fermi level after doping of yttrium oxide in ZrO_2, and the effect of doping on their stabilization are still not sufficiently understood due to the difficulty of detecting them in the experiment.

2. Ab-initio simulation details

Ab initio calculations were carried out on the basis of the density functional theory [20]. All three modifications of ZrO_2 (Fig. 1(a-c)) were first relaxed using the GGA functionals (PBE) [21] and strictly bounded normalized potential (SCAN) [22]. To obtain the most accurate value of the ground state energy, the total energy was calculated in terms of the GGA exchange correlation potential, and SCAN was used to correctly estimate the lattice parameters. The calculations were carried out using the Vienna Ab-initio Simulation Package (VASP 6.4.2) [23]. By comparing the total energy in the unit cell, the stability of the three phases of ZrO_2 was evaluated, and then a supercell with a size of 2x2x2 was created to simulate the effect of 3.23, 6.67, 10.34, and 16.15 mol% Y_2O_3 on the stability of ZrO_2 in

order to investigate doped-induced phase transitions of zirconium dioxide and evaluate the effect of Y_2O_3 doping on the position of the Fermi level, as well as the stability of this ZrO_2.
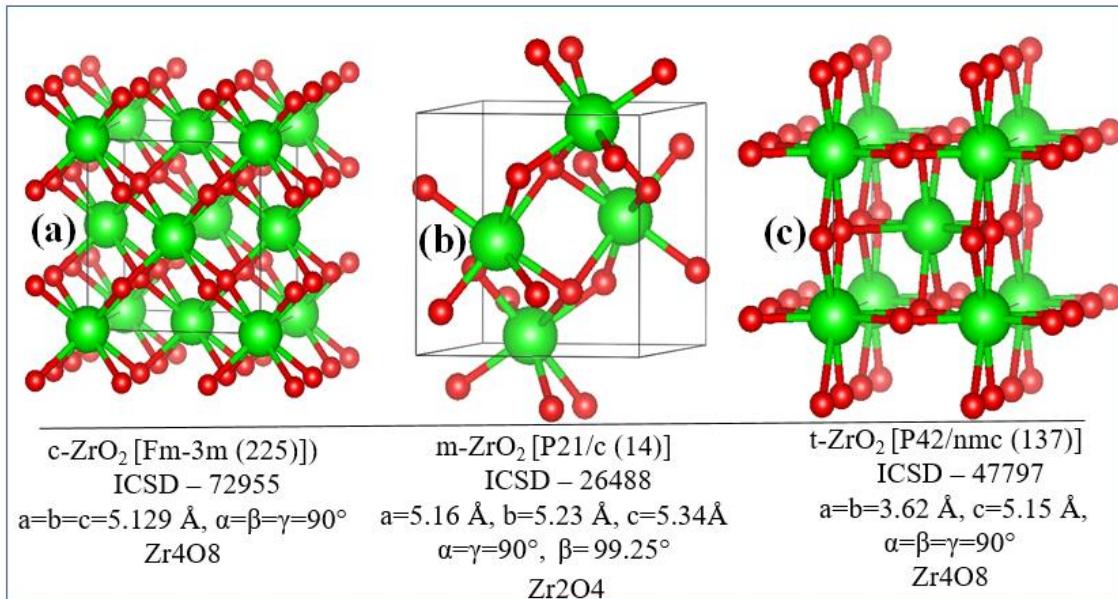
Figure 1. Crystal lattice models: a) cubic, b) monoclinic and c) tetragonal phase of ZrO_2.

For yttrium oxide doping, some Y_2O_3 formula units were replaced by ZrO_2 in a 2x2x2 supercell, with one oxygen vacancy created in each substitution. A schematic description of the generation of YSZ - structures is made according to the scheme:

$$xZrO_2 + kY_2O_3 \rightarrow Zr_xY_{2k}O_{2x+3k} + V_{o_k}$$
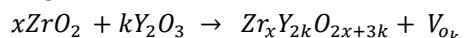
$$\%Y_2O_3 = \frac{k}{x+k} \times 100\% \qquad (1)$$

This can be thought of as combining x ZrO_2 formula units with k Y_2O_3 formula units arranged in an initial lattice of $x + k$ ZrO_2 units, resulting in the formation of m oxygen defects. Based on this, we determine the percentage of vacancy equal to the percentage of yttrium units in the final structure. Thus, our calculations were implemented for 4 different concentrations of Y_2O_3 doping (Table 1), which were refined using formula 1.

Table 1. Number of Zr, Y, O ions and oxygen vacancy for various mol. % Y_2O_3.

mol. %Y_2O_3	Zr	Y	O	O vacancy	System
0	32	0	64	0	Zr32O64
3.23	30	2	63	1	Zr30Y2O63
6.67	28	4	62	2	Zr28Y4O62
10.35	26	6	61	3	Zr26Y6O61
16.15	22	10	59	5	Zr22Y10O59

Vacancies were taken into account by removing one O atom with each subsequent substitution of 2 Y^{3+} ions in the Zr^{4+} position. The atomic orbitals O (2s, 2p), Zr (4d, 5s) and Y (4s 4p 4d 5s) were considered as valence electrons, while the remaining electrons were considered as nucleus electrons and remained frozen. The PAW method has been used to describe the interaction between valence electrons and electrons in the nucleus. The cutoff of the kinetic energy was fixed at the level of 600 eV, and all calculations were carried out taking into account spin-polarized effects. Orbital analyzes were performed by summing the contributions of individual atomic varieties in the unit cell and showing the contributions of the main atoms at the meeting point of the valence band and the conduction band.

3. Results and discussion

3.1. Structural, electronic and phonon properties of ZrO₂

At the first step of the study, the geometry of pure ZrO_2 phases was optimized using the VASP package. To find the optimal value of the cutoff energy (ENCUT) and the appropriate number of k-points in the Brillouin zone, we tested the convergence of the total unit cell energy as a function of ENCUT and KPOINTS. The results of the convergence test for the number of k-points for the ZrO2 cubic phase are shown in Figure 2, performed to build a k-point grid with a starting value of ENCUT = 1.3*ENMAX. Based on the results, it can be concluded that a 4x4x4 k-point grid with the Monkhrost-Pack scheme is optimally suited for the geometric relaxation of ZrO2. However, when calculating the electronic structure of these compounds, the number of k-points was at least doubled in order to obtain the most accurate density of states (DOS).
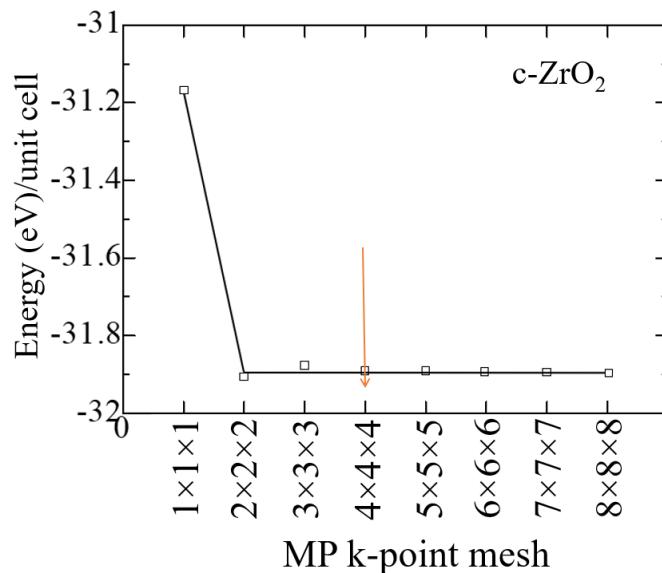
Figure 2. Total energy of the c-ZrO₂ unit cell as a function of the number of k-points (in the condition ENCUT=1.3*ENMAX).

Similar tests were carried out to establish the cutoff energy, from which it can be seen that the choice of ENCUT = 600 eV is suitable for modeling ZrO_2, and further increase in this energy only increases the calculation time without affecting its accuracy (Figure 3). Therefore, all further calculations were carried out at 600 eV. Similar convergence tests have also been carried out for the tetragonal and monoclinic phase of ZrO₂ using the GGA potential, which are also consistent with the results for the cubic phase.
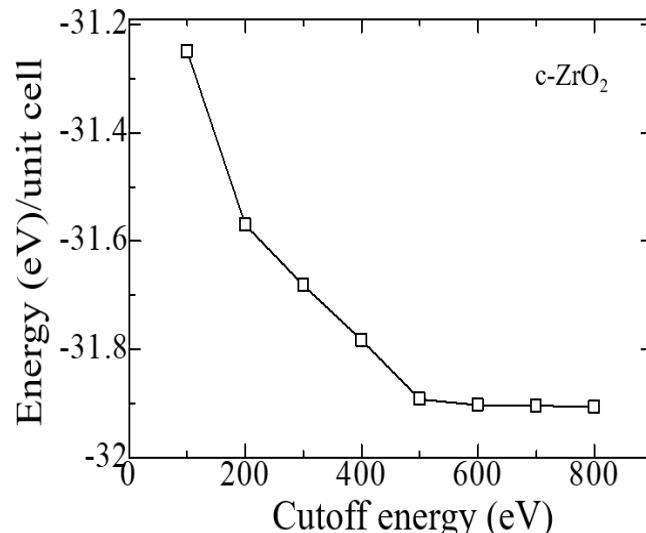
Figure 3. Total energy of the c-ZrO₂ unit cell versus cutoff energy (4 × 4 × 4 k-points).

Table 2 compares the calculated values of the lattice parameters of the ZrO₂ phase with the results from the literature.

Table 2. Relaxed parameters of the ZrO₂ phase (The calculated results are compared with experimental and previous theoretical results).

	Lattice constants	This work		Exp.
		GGA	SCAN	
m-ZrO₂ [P2_1/c]	a (Å)	5.191	5.115	5.0950[24]
	b (Å)	5.245	5.239	5.2116[24]
	c (Å)	5.202	5.304	5.3173[24]
	$\beta°$	99.639	99.110	99.230[24]
	V (Å³)	144.410	139.400	140.88[24]
t-ZrO₂ [P4_2/nmc]	a=b (Å)	3.593	3.622	3.64[25]
	c (Å)	5.193	5.275	5.27[25]
	c/a	1.445	1.456	1.45[25]
	V (Å³)	67.05	69.214	69.83[25]
	dz	0.012	0.013	0.046[25]
c-ZrO2 [Fm-3m]	a=b=c (Å)	5.075	5.12	5.129[26, 27]
	V(Å³)	130.709	134.06	134.9[26, 27]

According to the results given in Table 2, it can be seen that as the transition from a high-temperature phase to a lower-temperature phase, lattice distortion leads to a displacement of O ions in the c direction by a value of dz, expressed in relative units. As a result of distortion in the tetragonal phase, all Zr-O bonds will become nonequivalent. According to Table 2, the SCAN functionality describes the geometry much better than the standard GGA-PBE. Since the SCAN exchange-correlation functional describes the structural properties well, we decided to use this functional further when describing the geometry of other systems. The X-ray diffraction patterns of the initial structures obtained by us after their final relaxing are compared with the data from the literature, from which it can be seen that the results obtained by us are in good agreement with the experimental data, except for an imperceptible difference in the position of the X-ray peaks depending on the Bregg angles for the tetragonal system (Figure 4).
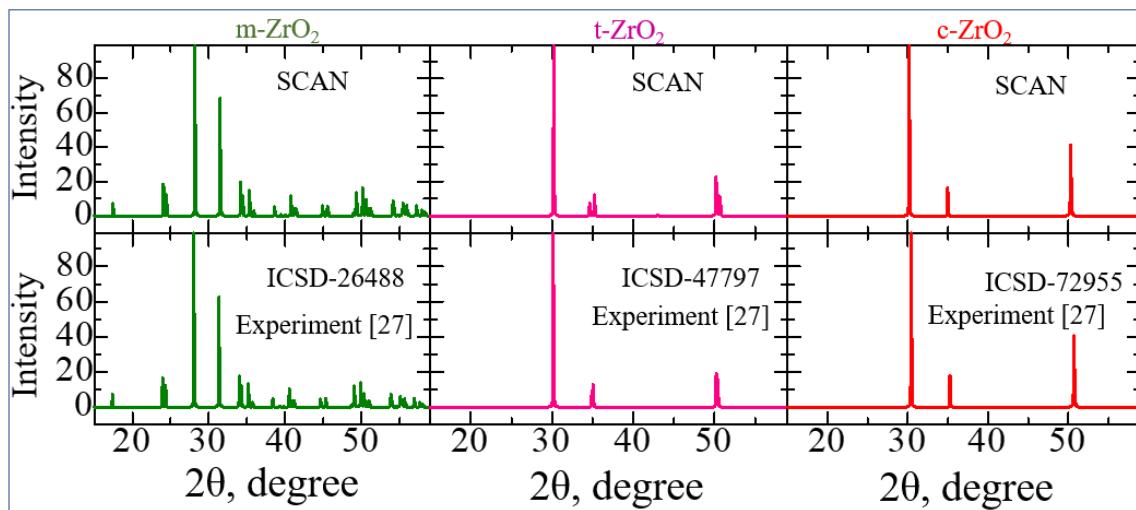
Figure 4. Comparison of experimental and calculated (SCAN) X-ray diffraction patterns of m-ZrO$_2$, t-ZrO$_2$, and c-ZrO$_2$.

Table 3 compares the total energy calculated by the GGA method for the monoclinic, tetragonal, and cubic ZrO$_2$ phases, from which it can be seen that m-ZrO$_2$ is the most stable phase in terms of energy values compared to other phases, that is, the monoclinic ZrO$_2$ phase with space group P21/ c is the most stable at low temperatures.

Table 3. GGA- calculated total electronic energies of c-ZrO2, t-ZrO$_2$, m-ZrO$_2$ unit cells.

System	Energy	ΔE
m-ZrO$_2$	**-28.7947**	**0**
t-ZrO$_2$	-28.6885	0.106
c-ZrO$_2$	-28.5865	0.201

Next, using the Phonopy code in the VASP package, we simulated the thermodynamic properties and phonon spectra of the ZrO$_2$ phase for a more detailed discussion of the structural stability of the ZrO$_2$ monoclinic phase. Figure 5 shows the change in the entropy of the unit cells of the ZrO$_2$ phase as a function of temperature.
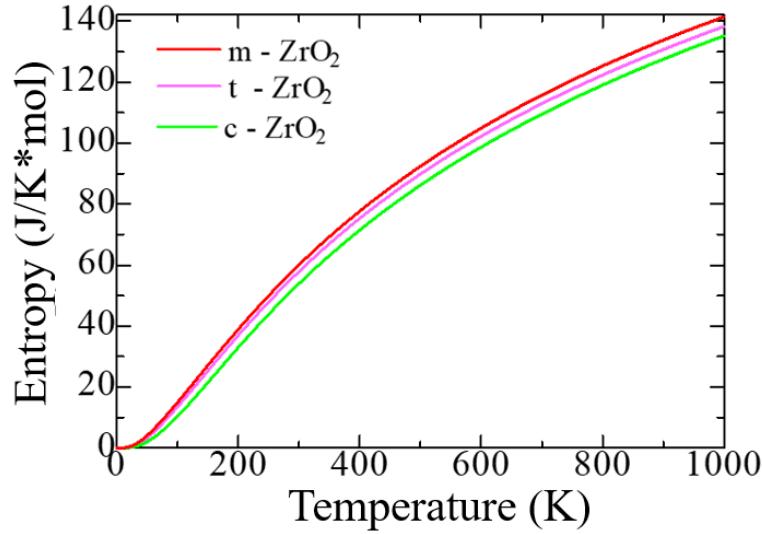
Figure 5. Entropy as a function of absolute temperature per unit cell c-ZrO$_2$, t-ZrO$_2$, m-ZrO$_2$.

According to Figure 5, as the transition from the monoclinic to the tetragonal and cubic phases, the entropy of these compounds decreases, which corresponds to the criterion of inverse dependence of enthalpy or direct dependence of the entropy and stability of solid systems [28]. This pattern can also be clearly observed after analyzing the pattern of phonon frequencies of the three phases of ZrO$_2$ (Figure 6 (a-c)) from which it is clearly seen that the monoclinic phase has the smallest negative modes than the other two phases.
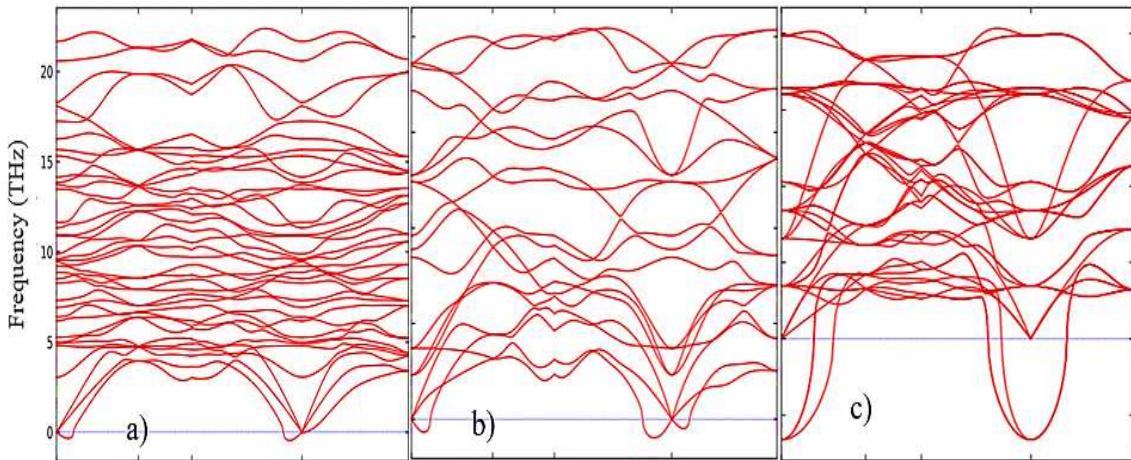
Figure 6. Phonon dispersion relations of (a) monoclinic, (b) tetragonal, and (c) cubic ZrO₂ at 0 K.

Figure 7(a-c) shows the temperature dependence of free energy, entropy and heat capacity for m-ZrO₂, t-ZrO₂ and m-ZrO₂.
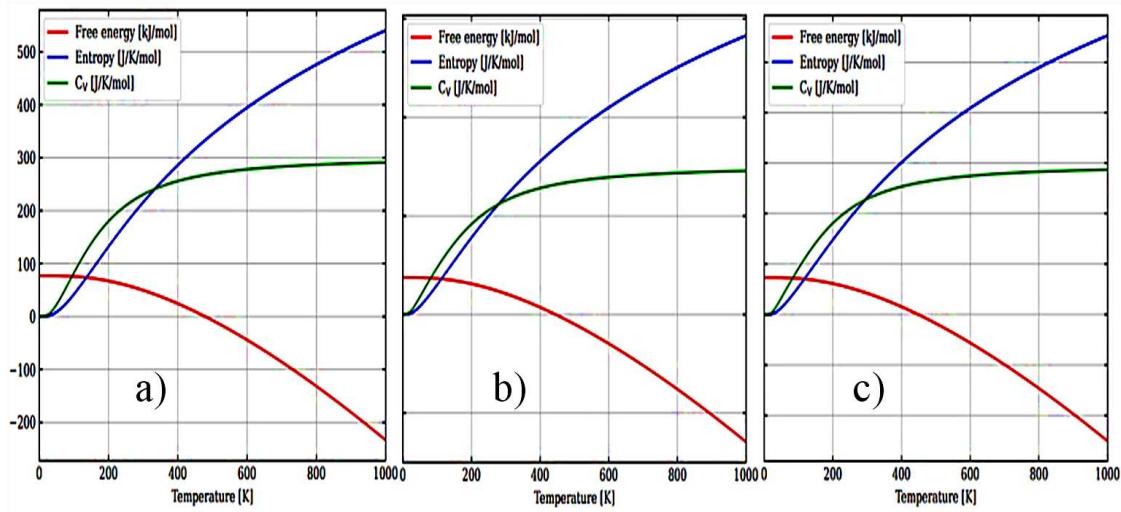
Figure 7. Temperature dependence of free energy, entropy and heat capacity for: m-ZrO₂ (a), t-ZrO₂ (b), and m-ZrO₂ (c).
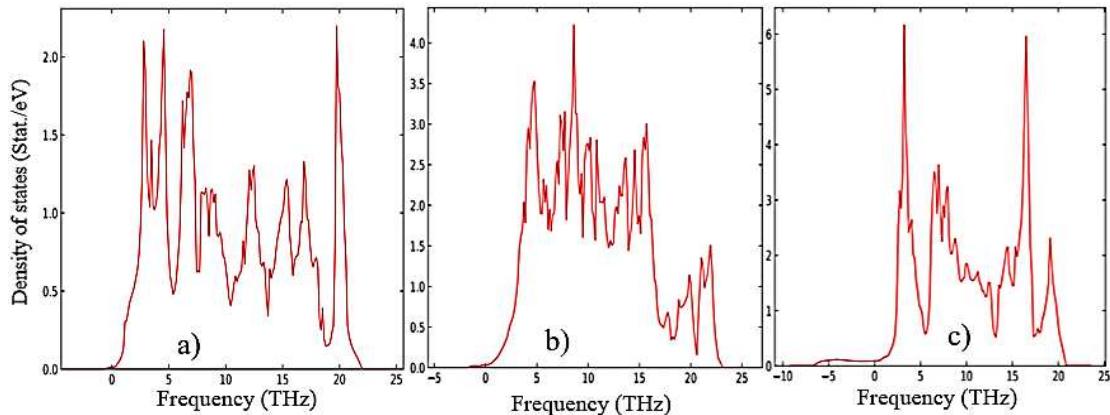
Figure 7. Phonon density of states for (a) m-ZrO2, (b) t-ZrO2, and (c) m-ZrO2.

The results of calculations of the density of phonon states are shown in Figure 7 (a-c) indicate that as the transition from the monoclinic to the tetragonal and cubic phases, the density of electronic states increases, and they also correspond well with the results given in Figure 6 and confirm the

monoclinic phase as the most stable among other ZrO_2 phases. This is also confirmed by the result of the Energy/Volume diagram shown in Figure 8 and is in good agreement with literature data [29]. Therefore, for further stabilization by doping with Y_2O_3, the choice of the monoclinic phase is appropriate.
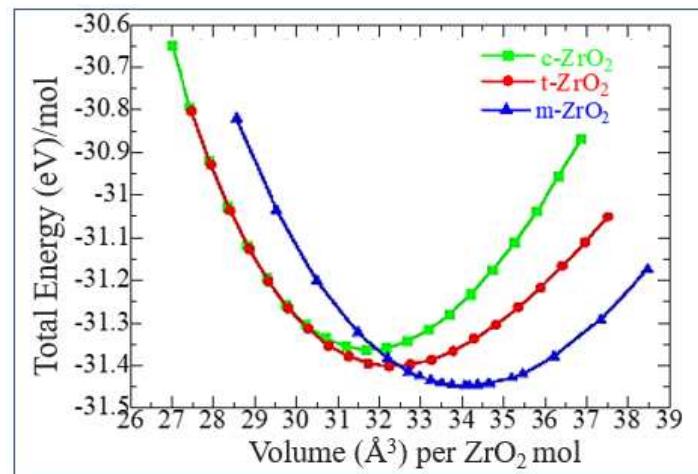
Figure 8. Total energy as a function of volume for m-ZrO_2 (a), t-ZrO_2 (b), and m-ZrO_2 (c).

Next, using the well-optimized structures of the three phases of ZrO_2, we studied the electronic properties of these systems. Using the GGA, SCAN functionals and the HSE06 hybrid functional, the band gap values of these systems were found (Table 4), their orbital structure was analyzed, and the change in the position of the Fermi level in these systems was modeled.

Table 4. Calculated and experimental band gap of c-ZrO_2, t-ZrO_2, m-ZrO_2 in eV.

System	This work			Experiment [30]
	GGA	SCAN	HSE06	
m-ZrO_2	3.9	3.8	5.288	5.78
t-ZrO_2	4.42	4.37	5.898	5.83
c-ZrO_2	4.03	3.93	5.140	6.10

According to the results presented in Table 3, the GGA and SCAN functionals showed a rather small band gap compared to the HSE06 hybrid functional [31], which traditionally overcomes underestimation of the band gap well. Given the suitability of HSE06 for estimating the band gap energy, we further used this particular hybrid functional to describe all problems related to the electronic properties of the systems under study.

Next, using the ZrO_2 structures relaxed using the SCAN functional, calculations were made of the density of available electronic states at the Fermi level (Figure 9), which is crucial for interpreting the electronic properties of ZrO_2 and the transport characteristics of electronic devices based on it.
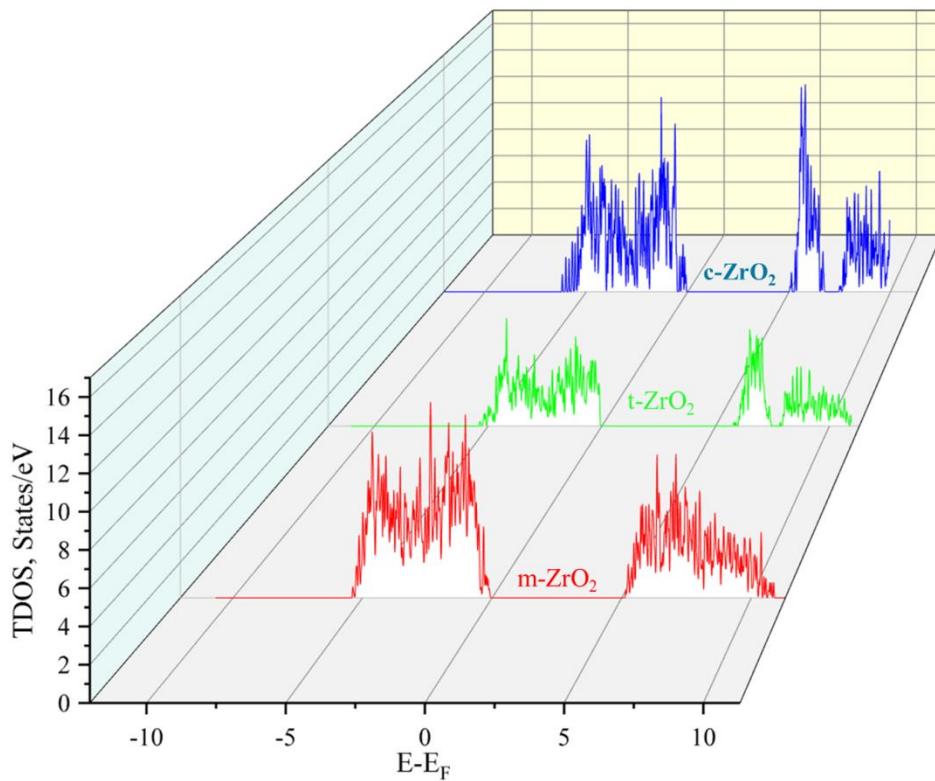
Figure 9. Total density of electron states (TDOS) of monoclinic, tetragonal, and cubic ZrO₂.

According to Figure 9, the density of electronic states for c-ZrO₂ is slightly overestimated compared to other phases. Moreover, secondary energy gaps are observed in the energy diagram of the tetragonal and cubic phases. Also, this gap increases with the transition from the tetragonal to the cubic phase.
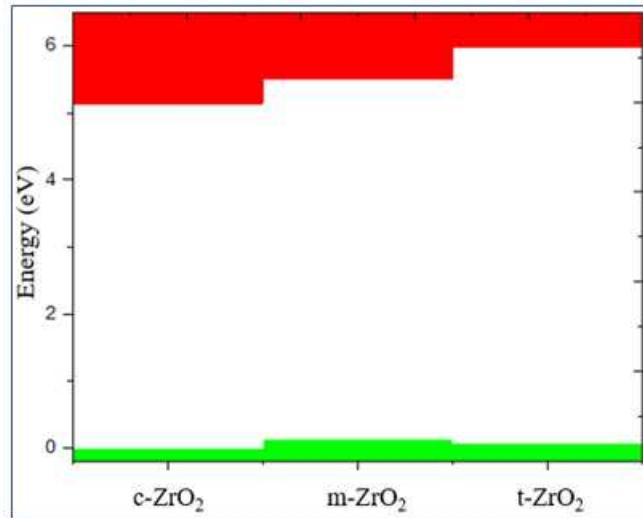
Рисунок 10. Conduction (red) - and valence (green)-band change for c-ZrO₂, t-ZrO₂, m-ZrO₂. Position of the Fermi level corresponds to the maximum of the valence band at each of the sites.

Next, we determined the position of the Fermi level in ZrO₂ crystals and the shift of this level during their phase transformation. As can be seen from Figure 10, if the position of the Fermi level (maximum of the valence band) for the monoclinic phase is taken as the reference point, then during the m-t phase transformation of ZrO₂, this level first drops by 0.125 eV towards lower energies and then descends again in the t-c section by 0.08 eV. This is also observed in detail from the results of the summarized bands for the orbital analysis, which are shown in Figure 11 for the three phases of ZrO₂.
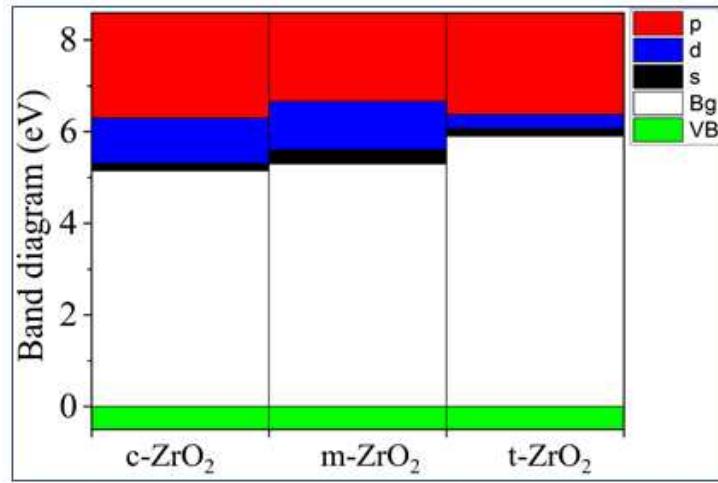
Figure 11. Composite PDOS diagram showing the main contributions of s-, p- and d-orbitals to the states that form the CB bottom for c-ZrO_2, t-ZrO_2, m-ZrO_2. Top of VB (green), scaled to zero.

It can be seen from Figure 11 that as we move from the monoclinic to the tetragonal and cubic phase, the contribution of the p orbitals becomes more significant in CB, and the s orbitals make a small contribution, while the d state shows a different trend. It is assumed that this behavior may be associated with a change in the crystal field and covalence of ZrO_2 during the phase transformation.

3.2. Stabilization of m-ZrO_2 and electronic properties of YSZ

After the final preparation of YSZ - structures (according to the scheme proposed in formula 1 and table 1), geometric optimization was carried out and Y_2O_3 - doped ZrO_2 supercells were relaxed using the GGA and SCAN functionals. Table 5 shows the geometric parameters of the ZrO_2 and YSZ supercells at various Y_2O_3 concentrations after relaxation using the SCAN functional.

Table 5. Lattice parameters of 2x2x2 supercells of ZrO_2 and YSZ at various Y_2O_3 concentrations.

System	Lattice parameters						Phase
	a (Å)	b (Å)	c (Å)	α (°)	β (°)	γ (°)	
0	10.23	10.478	10.608	90	99.64	90.00	m - YSZ
3.23 mol. %Y_2O_3	10.274	10.524	10.536	90.21	98.84	89.94	m - YSZ
6.67 mol. %Y_2O_3	10.512	10.544	10.603	89.90	90.12	89.62	t - YSZ
10.35 mol. %Y_2O_3	10.529	10.541	10.546	89.98	90.09	90.08	t - YSZ
16.15 mol. %Y_2O_3	10.540	10.541	10.543	90.08	90.00	90.02	c - YSZ

According to the results shown in Table 5, it can be seen that the doping of yttrium oxide, namely the concentration of more than 14 mol. %Y_2O_3 stabilizes the monoclinic phase of zirconia to a cubic phase. However, in this case, the lattice parameters of Y_2O_3 - doped structures change non-linearly. Figure 12 shows the volume vibration of ZrO_2 lattices as a function of Y_2O_3 concentration (x).
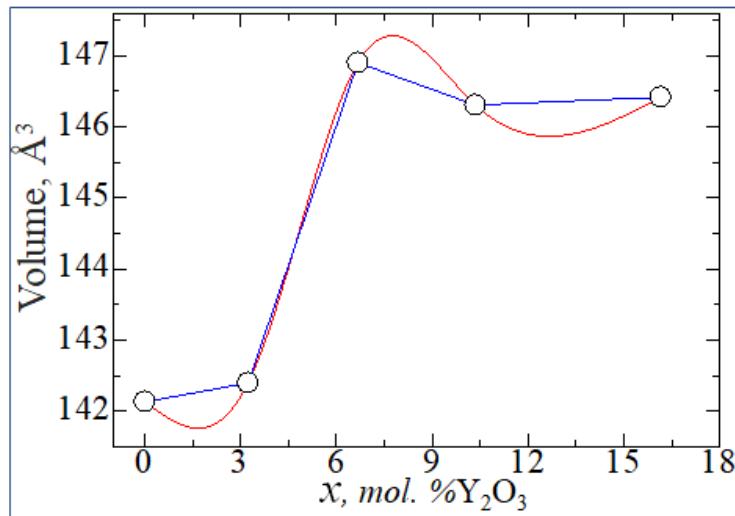
Figure 12. Vibrations of ZrO₂ volume as a function of Y₂O₃ concentration.

According to Fig. 13, with increasing doping concentration, the energy difference between the monoclinic phase with the tetragonal and cubic decreases, which indicates the possibility of doping-induced phase transitions of zirconium dioxide in the indicated Y₂O₃ doping concentration ranges.
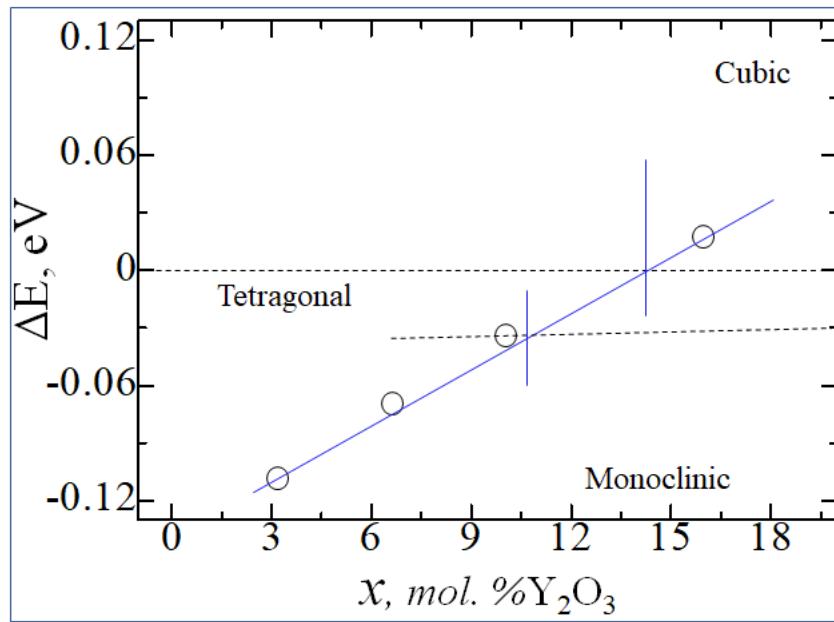
Figure 13. Total energy difference between unit cell phases of ZrO₂ as a function of Y₂O₃ doping concentration.

Having obtained the optimized structures, we calculated the energy of formation (E_f) and enthalpy energy of formation (ΔH) for ZrO₂ and YSZ, as well as the energy of formation of a vacancy (E_{df}) for YSZ using the following formulas:

$$E_f = E_{tot} - \sum_x E_{tot}(x) \tag{2}$$

$$E_{df} = E_{tot}^{Zr_{32-x}Y_xO_{64-\delta}} - E_{tot}^{Zr_{32}O_{64}} + \delta * E_{tot}^{O} \tag{3}$$

$$\Delta H = \frac{E_{YSZ} - [xE_{ZrO_2} + kE_{Y_2O_3}]}{x+k}, \tag{4}$$

where E_{tot} is the total energy of the system, $E_{tot}(x)$ is the total energy of individual components, and δ is the number of vacancies (defects) in the crystal. The calculated values of E_f and E_{df} per atom are given in Table 6.

Table 6. GGA-calculated values of enthalpy (ΔH) and formation energy (E_f) for ZrO_2 and YSZ. Oxygen vacancy formation energy (E_{df}) for YSZ.

System	ΔH	Ef	Edf
0	64.02917222	-4.747216667	0
3.23 mol. %Y_2O_3	59.91124404	-4.848422632	-1.874577368
6.67 mol. %Y_2O_3	56.13271879	-4.967857447	-3.739875532
10.35 mol. %Y_2O_3	52.7041267	-5.106527419	-5.596013441
16.15 mol. %Y_2O_3	47.00229139	-5.384704945	-9.220196154

On fig. Figure 14 shows a diagram of the dependence of the change in the enthalpy of formation of YSZ on the concentration of Y_2O_3, calculated by formula 4, from which it is clearly seen that doping with Y_2O_3 reduces the enthalpy and leads to the stabilization of zirconium dioxide. The empirical formula obtained by the least squares method says that the enthalpy of formation energy decreases linearly according to the law ΔH = -1.0407x + 63.532, where x is the concentration of Y_2O_3 in YSZ.
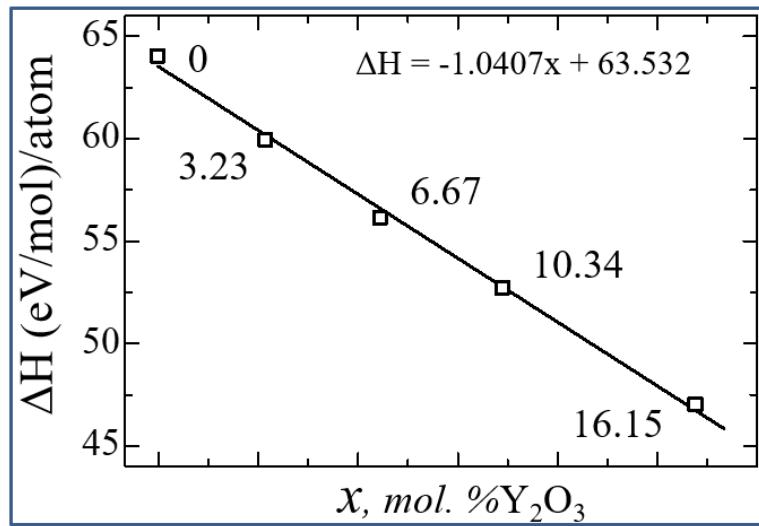
Figure 14. Enthalpy formation energy for YSZ as a function of Y_2O_3 concentration.

Thus, as the concentration of Y_2O_3 increases, the number of oxygen vacancies in YSZ increases, and the growth of these O vacancies is considered as a stabilizing mechanism for the monoclinic phase of zirconia, as evidenced by a decrease in the enthalpy of formation. The numerical value of the enthalpy formation energy is shown in Table 6.

Figure 15 shows the nature of the change in E_f and E_{df} from the concentration of yttrium oxide, from which the regularity of their linear decrease is clearly visible.
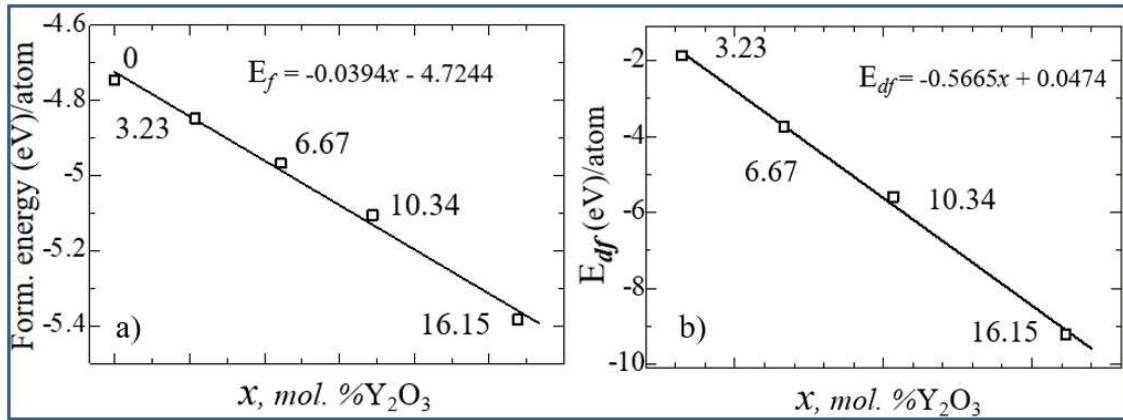
Figure 15. Energy of formation (a) and energy of formation of an oxygen vacancy (b) for YSZ as a function of Y_2O_3 concentration.

Next, calculations were carried out to study the electronic structure of Y_2O_3 stabilized ZrO_2 supercells to reveal in detail the effects of doping on their density of states, Fermi energy behavior, and orbital states. Figure 16 shows plots of the change in the density of electronic states YSZ for all doping concentrations of Y_2O_3.
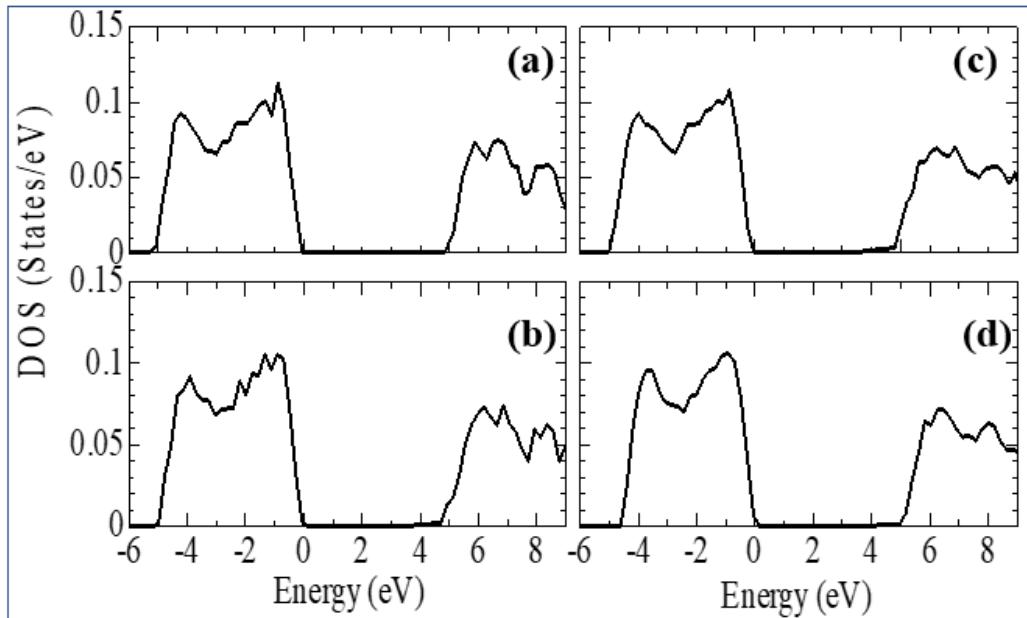
Figure 16. Total electron density of states (TDOS) for ZrO_2 doped with 3.23, 6.67, 10.34, and 16.15 mol% Y_2O_3.

According to the results presented in Figure 16, it can be seen that after Y_2O_3 doping in TDOS structures, no new energy states arise due to the introduction of defects, that is, it does not lead to a change, except for the band gap shift, which can be considered in detail after orbital analysis (Fig. 17) and estimates of the shift of the Fermi level (Fig. 18). The band gap is 4.71 eV, 4.92 eV, 4.75 eV, and 4.72 eV, respectively, for ZrO_2 with dopid 3.23, 6.67, 10.34, and 16.15 mol% Y_2O_3.
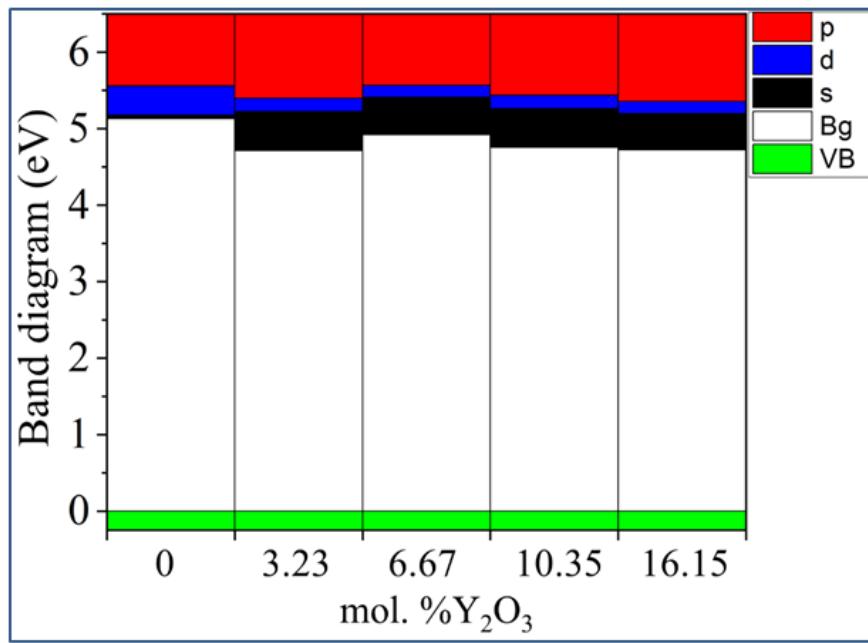
Figure 17. Composite PDOS diagram demonstrating the main contributions of s-, p- and d-orbitals to the states forming the CB bottom for ZrO_2 doped with 3.23, 6.67, 10.34 and 16.15 mol% Y_2O_3. Top of VB (green), scaled to zero.
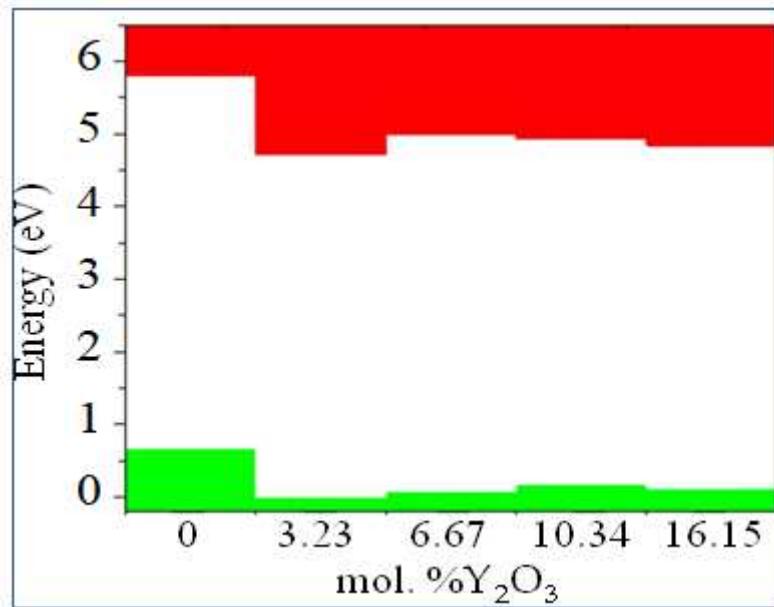
Figure 18. Conduction (red) - and valence (green)-band change for ZrO_2 doped with 3.23, 6.67, 10.34 and 16.15 mol% Y_2O_3. The position of the Fermi level corresponds to the maximum of the valence band at each of the sites.

According to Figure 18, after doping with 3.23 mol% Y_2O_3 in pure m-ZrO_2, the Fermi level drops by 0.067 eV and then shifts by 0.007 eV towards the conduction band when doped with 6.67 mol% Y_2O_3. Then, at a doping concentration of 10.34 mol%, it still rises by 0.01 eV, being 0.017 eV higher than in the case of 3.23 mol% Y_2O_3. However, after doping with 16.15 mol% Y_2O_3, it drops to 0.012 eV. According to the PDOS diagram, one can interpret and observe the step pattern of the conduction band with the contribution of s-, p- and d-orbitals. Understanding these features make it possible to tune the Fermi energies in the band structure for specific tasks in modern materials science and instrumentation. The results obtained will help to interpret some of the features of the electronic properties of ZrO2 and solid materials [32-48], and also complement the base of scientific work

carried out in the field of using biocompatible zirconium dioxide crystals and ceramics for generating green energy. The data can be used in the design of moisture-to-electricity converters and the creation of solid oxide fuels. cells based on ZrO_2 .

4. Conclusion

The phase transition of zirconia caused by yttrium doping leads to the stabilization of zirconia, which is widely used in many applications. Our calculations have shown that ab initio research methods are able to describe the mechanism of phase transitions of materials under the action of doping. That is, this approach can be applied to study the effect of doping on other properties that are difficult to observe experimentally. Also, using ab initio calculations, one can well describe the effect of doping on the behavior of the Fermi level in crystals. This result confirms the possibility of predicting the effect of doping on other physical properties of the system within the framework of the density functional theory. Thus, the calculations showed that the presence of oxygen vacancies plays an important role in the phase transition and stabilization of ZrO_2. The results obtained enrich the data bank to improve understanding of the phase transitions of zirconium dioxide, and can also be used to correct the parameters of theoretical calculations to describe other properties of zirconium dioxide, which are still beyond the scope of quantum chemical modeling.

Funding: The research leading to these results has received funding from the European Union's Horizon 2020 research and innovation programme under the Marie Sklodowvska-Curie grant agreement 871284 project SSHARE.

References

1. Chu, S., Cui, Y., & Liu, N. (2016). The path towards sustainable energy. Nature Materials, 16(1), 16–22. doi:10.1038/nmat4834.
2. Chu, S., & Majumdar, A. (2012). Opportunities and challenges for a sustainable energy future. Nature, 488(7411), 294–303. doi:10.1038/nature11475.
3. Shen, D., Xiao, M., Zou, G., Liu, L., Duley, W. W., & Zhou, Y. N. (2018). Self-Powered Wearable Electronics Based on Moisture Enabled Electricity Generation. Advanced Materials, 30(18), 1705925. doi:10.1002/adma.201705925.
4. Shao, C., Ji, B., Xu, T., Gao, J., Gao, X., Xiao, Y., Zhao, Y., Chen, N., Jiang, L., & Qu, L. (2019). Large-Scale Production of Flexible, High-Voltage Hydroelectric Films Based on Solid Oxides. ACS Applied Materials and Interfaces, 11(34), 30927–30935. doi:10.1021/acsami.9b09582.
5. Yashima, M., Ohtake, K., Arashi, H., Kakihana, M., & Yoshimura, M. (1993). Determination of cubic-tetragonal phase boundary in Zr1− XYX O2− X/2 solid solutions by Raman spectroscopy. Journal of applied physics, 74(12), 7603-7605.
6. Yashima, M., Sasaki, S., Kakihana, M., Yamaguchi, Y. A. S. U. O., Arashi, H. A. R. U. O., & Yoshimura, M. A. S. A. H. I. R. O. (1994). Oxygen-induced structural change of the tetragonal phase around the tetragonal–cubic phase boundary in ZrO2–YO1. 5 solid solutions. Acta Crystallographica Section B: Structural Science, 50(6), 663-672.
7. Yashima, M., Kakihana, M., & Yoshimura, M. (1996). Metastable-stable phase diagrams in the zirconia-containing systems utilized in solid-oxide fuel cell application. Solid State Ionics, 86, 1131-1149.
8. Yashima, M., Ohtake, K., Kakihana, M., Arashi, H., & Yoshimura, M. (1996). Determination of tetragonal-cubic phase boundary of Zr1− XRXO2− X2 (R= Nd, Sm, Y, Er and Yb) by Raman scattering. Journal of Physics and Chemistry of Solids, 57(1), 17-24.
9. Yashima, M., Ishizawa, N., & Yoshimura, M. (1993). High-Temperature X-ray Study of the Cubic-Tetragonal Diffusionless Phase Transition in the ZrO2─ ErO1. 5 System: I, Phase Change between Two Forms of a Tetragonal Phase, t′-ZrO2 and t ″-ZrO2, in the Compositionally Homogeneous 14 mol% ErO1. 5-ZrO2. Journal of the American Ceramic Society, 76(3), 641-648.
10. Leger, J. M., Tomaszewski, P. E., Atouf, A., & Pereira, A. S. (1993). Pressure-induced structural phase transitions in zirconia under high pressure. Physical Review B, 47(21), 14075.
11. Liu, L. G. (1980). New high pressure phases of ZrO2 and HfO2. Journal of Physics and Chemistry of Solids, 41(4), 331-334.
12. Yashima, M., Mitsuhashi, T., Takashina, H., Kakihana, M., Ikegami, T., & Yoshimura, M. (1995). Tetragonal─monoclinic phase transition enthalpy and temperature of ZrO2-CeO2 solid solutions. Journal of the American Ceramic Society, 78(8), 2225-2228.
13. Du, Y., Jin, Z., & Huang, P. (1991). Thermodynamic Assessment of the ZrO2─ YO1. 5 System. Journal of the American Ceramic Society, 74(7), 1569-1577.

14. Yashima, M., Hirose, T., Katano, S., Suzuki, Y., Kakihana, M., & Yoshimura, M. (1995). Structural changes of ZrO 2-CeO 2 solid solutions around the monoclinic-tetragonal phase boundary. Physical Review B, 51(13), 8018.

15. Clearfield, A. (1964). Crystalline hydrous zirconia. Inorganic Chemistry, 3(1), 146-148.

16. Doroshkevich, A. S., Nabiev, A. A., Pawlukojć, A., Doroshkevich, N. V., Rahmonov, K. R., Khamzin, E. K., ... & Ibrahim, M. A. (2019). Frequency modulation of the Raman spectrum at the interface DNA-ZrO 2 nanoparticles. Egyptian Journal of Chemistry, 62(2), 13-20.

17. A. Kvist, in: Physics of Electrolytes, Vol. 1, ed. J. Hladik (Academic Press, London, 1972) p. 319.

18. Lughi, V., & Sergo, V. (2010). Low temperature degradation-aging-of zirconia: A critical review of the relevant aspects in dentistry. Dental materials, 26(8), 807-820.

19. Kobayashi, K., Kuwajima, H., & Masaki, T. (1981). Phase change and mechanical properties of ZrO2-Y2O3 solid electrolyte after ageing. Solid State Ionics, 3, 489-493.

20. Hohenberg, P., & Kohn, W. (1964). Inhomogeneous electron gas. Physical review, 136(3B), B864.

21. Perdew, J. P., Burke, K., & Ernzerhof, M. (1996). Generalized gradient approximation made simple. Physical review letters, 77(18), 3865.

22. Sun, J., Ruzsinszky, A., & Perdew, J. P. (2015). Strongly constrained and appropriately normed semilocal density functional. Physical review letters, 115(3), 036402.

23. Kresse G, Furthmuller J. Efficiency of ab-initio total energy calculations for metals and semiconductors using a plane-wave basis set. Comput. Mater. Sci. 1996; 6:15–50.

24. Howard, C. J., Hill, R. J., & Reichert, B. E. (1988). Structures of ZrO2 polymorphs at room temperature by high-resolution neutron powder diffraction. Acta Crystallographica Section B: Structural Science, 44(2), 116-120.

25. Teufer, G. (1962). The crystal structure of tetragonal ZrO2. Acta Crystallographica, 15(11), 1187-1187.

26. Martin, U., Boysen, H., & Frey, F. (1993). Neutron powder investigation of tetragonal and cubic stabilized zirconia, TZP and CSZ, at temperatures up to 1400 K. Acta Crystallographica Section B: Structural Science, 49(3), 403-413.

27. Martin, U., Boysen, H., & Frey, F. (1993). Neutron powder investigation of tetragonal and cubic stabilized zirconia, TZP and CSZ, at temperatures up to 1400 K. Acta Crystallographica Section B: Structural Science, 49(3), 403-413.

28. Pascal, R., & Pross, A. (2015). Stability and its manifestation in the chemical and biological worlds. Chemical Communications, 51(90), 16160-16165.

29. Teter, D. M., Gibbs, G. V., Boisen Jr, M. B., Allan, D. C., & Teter, M. P. (1995). First-principles study of several hypothetical silica framework structures. Physical Review B, 52(11), 8064.

30. Heyd, J., Scuseria, G. E., & Ernzerhof, M. (2003). Hybrid functionals based on a screened Coulomb potential. The Journal of chemical physics, 118(18), 8207-8215.

31. Verma P, Truhlar D. HLE16: A Local Kohn-Sham Gradient Approximation with Good Performance for Semiconductor Band Gaps and Molecular Excitation Energies. J. Phys. Chem. Lett. 2017;8:380–87. doi.org/10.1021/acs.jpclett.6b02757.

32. Asgerov, E.B.; Beskrovnyy, A.I.; Doroshkevich, N.V.; Mita, C.; Mardare, D.M.; Chicea, D.; Lazar, M.D.; Tatarinova, A.A.; Lyubchyk, S.I.; Lyubchyk, S.B.; Lyubchyk, A.I.; Doroshkevich, A.S. Reversible Martensitic Phase Transition in Yttrium-Stabilized ZrO2 Nanopowders by Adsorption of Water, Nanomaterials 2022, 12, 3, 435.

33. Nematov, D. D., Kholmurodov, K. T., Husenzoda, M. A, Lyubchyk, A., & Burhonzoda, A. S. (2022). Molecular Adsorption of H2O on TiO2 and TiO2: Y Surfaces. Journal of Human, Earth, and Future, 3(2), 213-222.

34. Nematov D. Influence of Iodine Doping on the Structural and Electronic Properties of CsSnBr3. International Journal of Applied Physics 2022; 7:36-47.

35. Nematov D, Kholmurodov K, Yuldasheva D, Rakhmonov K, Khojakhonov I. Ab-initio Study of Structural and Electronic Properties of Perovskite Nanocrystals of the CsSn[Br1−xIx]3 Family. HighTech and Innovation Journal 2022; 3:140-50.

36. Davlatshoevich D.N. Investigation Optical Properties of the Orthorhombic System CsSnBr3-xIx: Application for Solar Cells and Optoelectronic Devices. Journal of Human, Earth, and Future, 2021; 2, 404-411.

37. Davlatshoevich N. D, Ashur K, Saidali B.A, Kholmirzo Kh, Lyubchyk A, Ibrahim M. Investigation of structural and optoelectronic properties of N-doped hexagonal phases of TiO2 (TiO2-xNx) nanoparticles with DFT realization: Optimization of the band gap and optical properties for visible-light absorption and photovoltaic applications. Biointerface Research in Applied Chemistry 2022; 12:3836-48.

38. Nematov D, Burhonzoda A, Khusenov M. First Principles Analysis of Crystal Structure, Electronic and Optical Properties of CsSnI3–xBrx Perovskite for Photoelectric Applications. J. Surf. Invest. 2021; 15:532–533. doi.org/10.1134/S1027451021030149.

39. Nematov, D.D. Kh.T. Kholmurodov, S.Aliona, K. Faizulloev, V.Gnatovskaya,T. Kudzoev, "A DFT Study of Structure, Electronic and Optical Properties of Se-Doped Kesterite Cu2ZnSnS4 (CZTSSe)," Letters in Applied NanoBioScience, 2022, 12(3), p. 67.

40. Nematov D, Makhsudov B, Kholmurodov Kh, Yarov M. Optimization Optoelectronic Properties ZnxCd1-xTe System for Solar Cell Application: Theoretical and Experimental Study. Biointerface Research in Applied Chemistry 2023; 13:90.

41. Nematov, D., Burhonzoda, A., Khusenov, M., Kholmurodov, K., Doroshkevych, A., Doroshkevych, N., ... & Ibrahim, M. (2019). Molecular dynamics simulations of the DNA radiation damage and conformation behavior on a zirconium dioxide surface. Egyptian Journal of Chemistry, 62(The First International Conference on Molecular Modeling and Spectroscopy 19-22 February, 2019), 149-161.

42. Nematov, D. D., Burhonzoda, A. S., Khusenov, M. A., Kholmurodov, K. T., & Ibrahim, M. A. (2019). The quantum-chemistry calculations of electronic structure of boron nitride nanocrystals with density Functional theory realization. Egyptian Journal of Chemistry, 62(The First International Conference on Molecular Modeling and Spectroscopy 19-22 February, 2019), 21-27.

43. Nizomov Z, Asozoda M, Nematov D. Characteristics of Nanoparticles in Aqueous Solutions of Acetates and Sulfates of Single and Doubly Charged Cations. Arabian Journal for Science and Engineering 2022, 47, 1-7.

44. Danilenko, I., Gorban, O., Maksimchuk, P., Viagin, O., Malyukin, Yu., Gorban S., Volkova, G., Glasunova, V., Guadalupe Mendez-Medrano, M., Colbeau-Justin, Ch., Konstantinova, T., Lyubchyk, S. Photocatalytic activity of ZnO nanopowders: The role of production techniques in the formation of structural defects.

45. Catalysis Today 2019, 328, 99–104.

46. Danilenko, I., Gorban, O., da Costa Zaragoza de Oliveira Pedro, P.M, Viegas, J., Shapovalova, O., Akhozov, L., Konstantinova, T., Lyubchyk S., Photocatalytic Composite Nanomaterial and Engineering Solution for Inactivation of Airborne Bacteria, Topics in Catalysis 2021, 64, 772–779.

47. Dilshod, N., Kholmirzo, K., Aliona, S., Kahramon, F., Viktoriya, G., & Tamerlan, K. (2023). On the Optical Properties of the Cu2ZnSn [S1− xSex] 4 System in the IR Range. Trends in Sciences, 20(2), 4058-4058.

48. Petrov, E. G., Shevchenko, Y. V., Snitsarev, V., Gorbach, V.V., Ragulya, A. V., Lyubchik, S. Features of superexchange nonresonant tunneling conductance in anchored molecular wires, AIP Advances 2019, 9, 115120.